Published in final edited form as:
J Comp Neurol. 2009 June 10; 514(5): 507–517. doi:10.1002/cne.22051.

Complete 3-D visualization of primate striosomes by KChIP1 immunostaining

Shawn Mikula[1], **Sarah K. Parrish**[1], **James S. Trimmer**[1,2], and **Edward G. Jones**[1]

[1]Center for Neuroscience, University of California, Davis

[2]Department of Neurobiology, Physiology and Behavior, University of California, Davis

Abstract

High resolution 3D reconstruction and morphometric analysis of striosomes was carried out in macaque monkeys using immunocytochemistry for the Kv4 potassium channel subunit, KChIP1, a novel marker. The striosomes form a connected reticulum made up of two distinct planar sheets spanning several millimeters in the putamen, and long finger-like branches in the caudate nucleus and putamen. Although their spatial organization is variable, morphometric analysis of the striosomes, utilizing skeletonizations, reveals several quantitative invariant measures of striosome organization, including: 1) individual bifurcation-free striosome branches are 355±108.5 microns in diameter and 1013±751 microns in length, and are both lognormally distributed, and 2) striosome branches exhibit three pronounced orientation preferences that are approximately orthogonal. The former finding suggests a fundamental anatomical and functional component of the striatum, whereas the latter indicates that striosomes are more lattice-like than their spatial variability suggests. The perceived variable spatial organization of the striosomes in primates belies many invariant features that may reflect striatal function, development, and pathophysiology.

Keywords

potassium channel subunit; putamen; caudate nucleus; basal ganglia; matrix

Introduction

Modularity and chemical compartmentalization are prevalent throughout the brain, and are present in primate cortical areas such as V1 and V2, the barrel cortex of rodents, the presubiculum, the entorhinal cortex, as well as the superior colliculus, thalamus, and striatum. Chemical compartments and modules are often associated with segregation of function. Well known examples in the primate visual cortex are the V1 blobs, which are organized as a lattice of patches in tangential sections and are known to be involved in color vision (Livingstone and Hubel, 1984). One of the most striking examples of chemical compartmentalization occurs in the striatum, in structures called the striosomes (Graybiel and Ragsdale, 1978).

The striatum is implicated in a wide range of functions from motor control to addiction, and although appearing as a generally homogeneous cell mass in Nissl-stained material, is strikingly organized into two complementary chemical compartments known as the matrix and the striosomes when visualized by staining for markers such as acetylcholinesterase (Graybiel and Ragsdale, 1978), enkephalin, substance P, limbic system-associated membrane protein

Send correspondence to: Dr Edward G. Jones, Center for Neuroscience, University of California Davis, Davis CA 95618, Phone: 530-757-8747, Fax: 530-754-9136 ejones@ucdavis.edu.

(LAMP) (Prensa et al., 1999), AMPA receptor subunit 1 (GluR1) (Martin et al., 1993), dopamine receptor subunits, and calcium binding proteins (O'Kusky et al., 1999). Striosomal abnormalities have been associated with neurological disorders, such as mood dysfunction in Huntington's disease (Tippett et al., 2007). Previous studies of the three-dimensional organization of the striosome system in cats and rats concluded that striosomes are organized as a reticulum (Desban et al., 1989; Desban et al., 1993; Groves et al., 1988; Manley et al., 1994). The detailed structure of primate striosomal organization has not been described.

In the current study, we used immunocytochemical localization of KChIP1 (voltage-gated potassium channel interacting protein 1), a calcium-binding protein that interacts with transient voltage-gated potassium channel, localized in neuronal somata and dendrites (Rhodes et al., 2004), to modulate neuronal excitability (An et al., 2000; Beck et al., 2002). This gave a high contrast view of the striosomes in Old World monkeys that permitted more accurate reconstruction than hitherto possible.

Material and Methods

Antibody characteristics

Anti-Calbindin. A rabbit anti-calbindin antibody, kindly provided by Dr. P. C. Emson, Brabraham Institute, Cambridge, UK, was used to stain the complementary matrix compartment in the striatum. The antiserum was produced against calbindin, M.W. 28,000, purified by high-pressure liquid chromatography after isolation from chick intestine (Spencer et al., 1978). Western blotting has shown that the antiserum specifically recognizes calbindin of molecular weight 28,000 in macaque brain (Graziano and Jones, 2004). Immunostaining patterns obtained in the present study were consistent with those previously reported in previous studies using this antibody in Old World monkeys (e.g. Jones and Hendry, 1989; Graziano and Jones, 2004).

Anti-KChIP1. Purified mouse monoclonal anti-KChIP1 antibody, K55/7 (available from the University of California, Davis NeuroMab Facility, www.neuromab.org), was used to stain striosomes. This monoclonal antibody was generated against a recombinant fusion protein containing full length (amino acids 1-216) rat KChIP1 (Menegola et al., 2008; Rhodes et al., 2004). In immunofluorescence and immunoblot assays K55/7 specifically recognizes recombinant rat KChIP1 but not rat KChIPs 2-4 expressed in heterologous cells (Rhodes et al., 2004). The rat KChIP1 sequence is 98% identical to *Macaca mulatta* KChIP1 and 99% identical to *Homo sapiens* KChIP1; the *Macaca fascicularis* KChIP1 sequence is not available.

Immunocytochemistry

Four cerebral hemispheres from three male cynomolgus monkeys (*M. fascicularis*) were used. The brains were fixed by perfusion with 4% paraformaldehyde in 0.1M phosphate buffer, frozen in dry ice and sectioned on a sliding microtome. Both hemispheres from one monkey (cases 91L and 91R) were cut coronally at 25 microns. The right hemisphere of a second monkey (case 76R) was cut coronally at 30 microns. The left hemisphere of a third monkey (case 111R) was blocked just posterior to the anterior commissure, and cut at 30 microns in an oblique plane parallel to the internal capsule, approximately midway between the sagittal and horizontal planes. The 3D reconstruction for case 111R was limited to the head of the caudate nucleus and was used to confirm the qualitative and quantitative results from the three complete reconstructions (Cases 76R, 91L, and 91R); however, this case is not included in the Results section due to it being an incomplete reconstruction of the striosomes and striatum. The section thickness does not factor into the various morphometric calculations, and is only used for correctly scaling the 3D reconstructions and skeletonizations (see below). Sections were pre-incubated for 10 mins in a 1:1 mixture of 0.1 M phosphate buffer (PBS) and ethanol containing

1% hydrogen peroxide to block endogenous peroxidase that might contribute to background staining, followed by three rinses through PBS, and then 1 hr in blocking solution (BS) containing 3 percent normal serum and 0.25 percent Triton X-100 in 0.1M PBS. Every sixth regularly-spaced section was incubated for 48hr at 4°C in BS containing KChIP1 monoclonal antibody at 1:1000. Adjacent sections were incubated for 48hr at 4°C in BS containing D-28k calbindin rabbit polyclonal antibody at 1:2000; calbindin immunoreactivity is a known marker for the complementary matrix compartment. After three washes in PBS, the sections were incubated in BS containing biotinylated secondary antibody (1:200) for 1 to 2 hr., washed three times in PBS, and transferred to PBS containing the peroxidase conjugate from the Vectastain ABC kit (Vector Laboratories, Burlingame, CA). After rinsing three times in PBS, the sections were immersed in a solution of 0.02% 3-3′ diaminobenzidine-4HCl (DAB, Sigma-Aldrich, St Louis, MO) and 0.003% hydrogen peroxide. After staining, the sections were mounted on gelatinized glass slides, dehydrated in increasing concentrations of ethanol, cleared in xylene and coverslipped with DPX medium. Several unstained sections were mounted on glass slides for purposes of comparison with immunocytochemically processed sections, in order to compute shrinkage factors due to immunocytochemical processing.

Image Acquisition

Glass-mounted sections were scanned at 20× (0.46 um/pixel) in an Aperio ScanScope T3 scanner (Aperio Technologies, Vista, CA), specially adapted to accommodate 3″×2″ slides, to generate virtual (i.e., digital) slides and subsequently uploaded to the publicly-accessible BrainMaps.org server (Mikula et al., 2007). All image data used in this study can be accessed and downloaded from www.BrainMaps.org.

3D Reconstruction

3D reconstruction involved striosome segmentation (Fig. S1), image alignment, isosurface extraction, and surface rendering. The total number of sections used for 3D reconstructions is as follows: 1) case 76R, 92 sections at 30 micron thickness, 2) case 91L, 99 sections at 25 micron thickness, 3) case 91R, 99 sections at 25 micron thickness, and 4) case 111R, 33 sections at 30 micron thickness. Gradients in the immunostained striatal neuropil invalidated striatal and striosomal segmentations relying on global thresholds, and so semi-manual segmentation was employed using the tracing or magic wand tools in Photoshop CS3 (Adobe Systems Inc., San Jose, CA) and validated with manual inspection. RGB images were constructed so that the first channel contained the grayscale image of the entire section, the second channel contained the segmented striatum, and the third channel contained the segmented striosomes. Automated rigid body image alignments of the RGB images was performed in ImageJ (Rasband, 1997) using the plug-in, StackReg, that implements a pyramid approach to subpixel registration based on pixel intensity (Thevenaz et al., 1998). Three-dimensional volumetric reconstructions were performed using Isosurf, a freeware program that uses regularized marching tetrahedra for iso-surface extraction (Treece et al., 1999) and were validated against volumetric renderings of the original aligned RGB image stack using Imaris, v5 (Bitplane AG, Zurich, Switzerland). Three-dimensional reconstructions, using the extracted isosurfaces, were rendered in Lightwave 3D, v9.3.1 (Newtek Inc., San Antonio, TX).

Spatial Averaging across Striosomes

Grayscale (intensity) and binary image stacks of the striosomes from cases 76R, 91L, and 91R were rigidly aligned in ImageJ, and subsequently imported into Matlab (Mathworks Inc., Natick, MA) for spatial averaging, which consisted of computing intensity and binary products on a voxel-wise basis. Computation of percentage of striosome overlap utilized the spatially registered binary image stacks. Visualization of results was performed in Imaris, v5 (Bitplane AG, Zurich, Switzerland).

Skeletonization and Morphometric Analysis

Striosome image stacks were down sampled to generate voxel sizes of 110×110×150 microns for cases 91L and 91R and 110×110×180 microns for case 76. Skeletonization of the 3D striosome volumes was performed in Imaris (Bitplane AG, Zurich, Switzerland) using the Autopath method for skeletonization, which is a 3D extension of the 2D method described in Meijering et al. (Meijering et al., 2004). This method uses spot objects, the starting point (large), and end points (small) are defined in the dataset volume. Then a Fast Marching algorithm is used to connect end points to the starting point, along the path of greatest intensity. The resulting skeleton is defined in terms of striosome segments connected by branch points. Skeletonizations were exported from Imaris and imported in Matlab for computation of skeleton branching angles, segment orientations (in spherical coordinates), segment lengths, and segment diameters using custom-coded scripts. Striosome orientations were binned into 5° theta and phi increments, in spherical coordinates, where theta is the angle that the projection of the striosome segment makes in the coronal plane and ranges from 0° to 360°, and where phi is the angle offset of the striosome segment from the coronal plane, and ranges from 0° to 90°. These binned striosome segmentations were subsequently mapped onto the sphere for visualization purposes.

Results

KChIP1 is a Novel Immunocytochemical Marker for the Striosomes in Macaque

KChIP1 is a remarkably clear-cut immunocytochemical marker for the striosomes in the macaque monkey (Fig. 1). Coronal sections at the level of the anterior commissure showing KChIP1 immunoreactivity in the striosomes (Fig 1a), when compared with adjacent sections stained for calbindin immunoreactivity, reveal (Fig. 1b) a striking complementarity: calbindin exhibits high immunoreactivity in the matrix compartment and KChIP1 in the striosome compartment of the caudate nucleus and putamen. There is no KChIP1 immunostaining of the nucleus accumbens which is more or less homogeneously immunoreactive for calbindin. In sections cut approximately parallel to the internal capsule (dashed line in Fig. 1a), a lattice-like pattern of KChIP1 immunoreactive striosomes is evident in the head of the caudate nucleus (Fig. 1c), with complementary immunostaining for calbindin seen in an adjacent section (Fig. 1d). Higher magnification reveals KChIP1 immunoreactivity of somata in both matrix and striosomes (Fig. 1c upper inset), but heavy immunoreactivity of the neuropil only in the striosomes (Fig. 1c lower inset). This neuropil immunoreactivity is made up of interlacing neuronal processes of large and small diameter on a diffusely immunostained background. Based on the somal diameter (10-15 microns) and morphology (including an apparent lack of dendritic spines) of the immunoreactive neurons, we believe that the KChIP1-immunoreactive somata may belong to the “aspiny type I” class of DiFiglia et al. (DiFiglia et al., 1976). preliminary results from double immunocytochemical staining for KChIP1 and calbindin (a marker for medium spiny projection neurons), or for KChIP1 and the striatal interneuronal markers, choline acetyltransferase (ChAT), neuropeptide-Y, parvalbumin and calretinin, have revealed no colocalization of KChIP1 and any of these markers (data not shown).

Three Dimensional Reconstructions and the Qualitative Organization of the Striosomes

In three dimensional reconstructions (Figs 2, 3), the striosomes occupy 15.85% of the volume of the striatum (caudate nucleus, putamen and nucleus accumbens), or 16.64% when the nucleus accumbens, which accounts for about 4.8% of the macaque striatum, is excluded; this agrees with previous estimates of 15% based on counting relative striosome areas in serial sections of enkephalin immunoreactive material (Johnston et al., 1990).

Three dimensional reconstructions demonstrate that the striosomes form a connected reticulum. Many striosomes extend from the putamen into the caudate nucleus through the

neuronal bridges in the internal capsule. These 'bridge' striosomes have an antero-dorso-medial to postero-ventro-lateral bias, the same as the neuronal bridges. The caudate striosomes are located predominantly in the head of the caudate nucleus and are organized as a series of serpentine, finger-like structures, which we call striosome branches; three-dimensional reconstructions demonstrate that the branches also have a pronounced antero-dorso-medial to postero-ventro-lateral bias, often running through the internal capsule into the putamen through the cell bridges. Striosomes are sparse in the body of the caudate nucleus and are absent from the tail. In the putamen, there is one striosomal sheet at the anterior pole of the putamen and a second in its lateral aspect, which extends through the anterior half of putamen, running parallel to the claustrum. Although these features of the putamen striosomes were constant across monkeys and cerebral hemispheres of the same monkey, there is considerable variability in their exact shape, as demonstrated in Figs 2c and 3c.

Spatial Averaging across Striosomes

Spatial averaging over all volumetric striosome data reveals markedly little overlap (<5%) due to variability in the shape of the striatum between animals, which results in poor rigid registration results (data not shown). Nevertheless, rigid registration of striata (and corresponding striosomes) from the two hemispheres of the same animal (cases 91L and 91R) produced a very good fit, and resulted in a 14.7% overlap between the striosomes in the two striata of the same animal (Fig. 4), with a large fraction of the overlap attributable to the striosomal sheet in the lateral putamen. Lesser disconnected regions of overlap were observed in the striosome branches.

Morphometrics and the Quantitative Organization of the Striosomes

Skeletonization of the striosomes, which preserves the overall morphology of the striosomes, and subsequent morphometric analysis, offers a way to bypass the difficulties encountered in spatial averaging across striosomes. Comparison of striata from hemispheres 76R, 91L, and 91R (Figs. 5, S2, and S3), revealed marked variability in the overall skeletonizations, and of the morphologies of different striosomes. By contrast, morphometric measures (Figs. 5, S2, and S3), including striosome segment orientations, bifurcation angles, striosome diameters and segment lengths, revealed a striking similarity.

For case 91R, bifurcation angles (n=878) had a mean of 87.3±31.6° (Fig. 5D). Striosome diameters (n=776) had a mean of 348.8±110.2 microns, and lengths (n=776) a mean of 1045.8 ±738.7 microns (Fig. 5E). These values are comparable to the corresponding values for cases 76R (Fig. S2) and 91L (Fig. S3).

Figure 6 shows group morphometric analyses of the three coronal cases (cases 76R, 91L, and 91R). Striosome segment orientations (Fig. 6A) and polar plots of the projection of the striosome orientations onto the coronal plane (Fig. 6B) revealed three prominent striosome orientation preferences in approximately orthogonal directions: posteromedial-to-anterolateral, anterodorsomedial-to-posteroventrolateral, and anteroventromedial-to-posterodorsolateral. Bifurcation angles (mean=84.6±33.7°, n=2764) are shown in 6C. Striosome diameters (mean=355.3±108.5 microns, n=2366), fit with a lognormal distribution, are shown in Fig. 6D. Striosome lengths (mean=1013.7±750.9 microns, n=2366), also fit with a lognormal distribution, are shown in Fig. 6E.

Discussion

The striosomes in the macaque are organized as a connected reticulum similar to that suggested for cats and rodents (Desban et al., 1989; Desban et al., 1993; Groves et al., 1988; Manley et al., 1994). The 3D reconstructions of the striosomes, made possible by the high resolution

immunostaining for KChIP1, revealed that within the connected reticulum the striosomes form planar sheets that can span several millimeters in the putamen, and long, serpentine, finger-like branches of ~1 mm in length in both the caudate nucleus and putamen. The striosome branches have a consistent anterodorsomedial-to-posteroventrolateral bias especially in the caudate nucleus. One striosome sheet is consistently observed at the anterior pole of the putamen and a second in the anterior half of putamen at its lateral-most edge running parallel to the claustrum.

The high variability in the spatial organization of the striosomes precluded useful analysis via spatial averaging across striosomes. Morphometric analyses, utilizing skeletonizations of the striosomes, however, revealed several quantitatively invariant measures of striosome organization: 1) individual striosome branches are 355±108.5 microns in diameter and are 1013 ±751 microns in length before giving rise to collateral branches, and are both lognormally distributed; 2) the bifurcation angle between striosome branches is 84.6±33.7° and is normally distributed; 3) striosome branch orientations exhibit pronounced biases in the posteromedial-to-anterolateral, anterodorsomedial-to-posteroventrolateral, and in the anteroventromedial-to-posterodorsolateral directions, approximately orthogonal directions that may have functional significance (see below).

Comparison with Previous Studies

Previous reconstructions of striosomes have depended upon their negative visualization in preparations in which the matrix compartment was stained. Full reconstructions of striosomes have been previously performed only in the rat (Desban et al., 1993), though partial reconstructions of those in the caudate nucleus have been done in cats (Desban et al., 1989; Groves et al., 1988; Manley et al., 1994). We did not find a continuous laminar (sheet-like) striosome along the anteroposterior extent of the dorsal caudate nucleus as described by Desban et al. (1989) in the cat. We believe their finding is likely due to incomplete staining of the matrix compartment, which may be brought about by fixative overexposure (Graybiel and Ragsdale, 1978) and thus incomplete visualization of the negatively stained striosomes. Other studies employing positive enkephalin immunostaining of the striosomes also failed to find a sheet-like striosome in the caudate nucleus (Groves et al., 1988). Desban et al (1989) also suggested that striosomes in the cat caudate nucleus resembled a continuous network of channels oriented in parallel arrays both in the rostrocaudal and mediolateral axis. Groves et al. (1988) found instead that the cat striosomes were organized as finger-like structures radiating ventrolaterally from the ventricular edge, connected to each other by smaller cross bridges (their Fig 6), which is consistent with the present results in the monkey.

Functional Implications

The observation that a typical striosome segment is 355 microns in diameter by 1 mm in length suggests that this is a fundamental anatomical and functional entity of the striatum, perhaps analogous to a cortical column (Mountcastle, 1997), although distributed in three dimensions in the striatal volume instead of across the thickness of the cortical sheet. The observation that striosome branches have three strong orthogonal orientation preferences suggests that the striosomes are organized as a lattice. The orthogonal orientation preferences of the striosomes suggests that different types of information could be mapped onto the three different directions, though physiological recordings or other high resolution neuronal mapping methods, would have to confirm this hypothesis. The mapping of different types of information onto orthogonal directions is a feature of primary visual, auditory, and somatosensory cortices (Linden and Schreiner, 2003), as well as other brain regions, so the three orthogonal orientation preferences of the striosomes is highly suggestive of a similar mapping process. Prelimbic prefrontal cortical areas (areas 25 and 32 in macaque) and midline thalamic nuclei, structures associated with self-monitoring and homeostasis, innervate the striosomes, whereas associational and

sensori-motor related prefrontal areas, and intralaminar thalamic nuclei, innervate the matrix (Donoghue and Herkenham, 1986; Gerfen, 1984; Ragsdale and Graybiel, 1991; Graybiel, 1995; Jones, 2007). Given the lack of direct connections of midline thalamic nuclei and prelimbic prefrontal areas with other sensori-motor-associational regions of cortex, the striosomes may play a major role in integrating information from these two sources by way of intrinsic striatal connections (Penny et al., 1988; Tepper et al., 2004). In this manner, prelimbic prefrontal areas and midline thalamic nuclei would be able to modulate sensori-motor-associational activities in other regions of the brain through their projections to the striosomes. By forming a connected reticulum throughout the striatum, the striosomes are in a position to modulate matrix activities throughout the striatum via intrinsic connections.

Certain inferences about physiological differences between the striosome and matrix compartments of the striatum can be drawn from the chemical localization of KChIP1 in the striosomal neuropil. KChIP1 is a member of the family of voltage-gated potassium (Kv) channel-interacting proteins (KChIPs, encoded by the KCNIP genes), which belong to the recoverin branch of the EF-hand superfamily of small calcium-binding proteins (An et al., 2000). Members of the KChIP family have highly-conserved core domains that contain EF-hand-like calcium binding motifs, and differ in their unique N-termini (An et al., 2000). KChIPs are component cytoplasmic subunits of native Kv4 channel complexes (Rhodes et al., 2004). Different KChIPs exhibit region and cell-type-specific associations with distinct Kv4 family members (Menegola et al., 2008; Menegola and Trimmer, 2006; Rhodes et al., 2004; Strassle et al., 2005), suggesting the distinct functional properties of specific Kv4:KChIP channel complexes observed in heterologous cells (Jerng et al., 2004) may have important functions in specific neuronal populations. In rat, KChIP1 is prominently expressed, along with the Kv4.3 primary subunit, in interneurons throughout the brain, while other Kv4 and KChIP subunit combinations predominate in principal cells (Menegola et al., 2008; Menegola and Trimmer, 2006; Rhodes et al., 2004; Strassle et al., 2005). Co-expression of KChIP1 and Kv4.3 includes a subset of interneurons in hippocampus (Menegola et al., 2008), cerebral cortex and striatum (Rhodes et al., 2004). The specific pairing of KChIP1 and Kv4.3 in interneurons suggests a specific but as yet uncharacterized role for this particular subunit combination in specific interneuron populations. KChIPs regulate the activity of the Kv4 channel complexes, which underlie somatodendritic A-type potassium currents, prominent in determining the interval between consecutive action potentials during repetitive firing, and hence neuronal excitability, in response to changes in intracellular calcium (An et al., 2000). The concentration of KChIP1 to the striosomal neuropil suggests that dendrites of neurons here possess functional properties distinct from those of cells in the surrounding matrix.

Supplementary Material

Refer to Web version on PubMed Central for supplementary material.

Acknowledgments

We thank Dr. Karl Murray for useful discussions over the neurochemical organization of the striatum. Supported by Grants Numbers MH60975, MH77556, and NS42225 from the National Institutes of Health, United States Public Health Service.

Literature Cited

An WF, Bowlby MR, Betty M, Cao J, Ling HP, Mendoza G, Hinson JW, Mattsson KI, Strassle BW, Trimmer JS, Rhodes KJ. Modulation of A-type potassium channels by a family of calcium sensors. Nature 2000;403:553–556. [PubMed: 10676964]

Beck EJ, Bowlby M, An WF, Rhodes KJ, Covarrubias M. Remodelling inactivation gating of Kv4 channels by KChIP1, a small-molecular-weight calcium-binding protein. J Physiol 2002;538:691–706. [PubMed: 11826158]

Desban M, Gauchy C, Kemel ML, Besson MJ, Glowinski J. Three-dimensional organization of the striosomal compartment and patchy distribution of striatonigral projections in the matrix of the cat caudate nucleus. Neuroscience 1989;29:551–566. [PubMed: 2739901]

Desban M, Kemel ML, Glowinski J, Gauchy C. Spatial organization of patch and matrix compartments in the rat striatum. Neuroscience 1993;57:661–671. [PubMed: 8309529]

DiFiglia M, Pasik P, Pasik T. A Golgi study of neuronal types in the neostriatum of monkeys. Brain Res 1976;114:245–256. [PubMed: 822916]

Donoghue JP, Herkenham M. Neostriatal projections from individual cortical fields conform to histochemically distinct striatal compartments in the rat. Brain Res 1986;365:397–403. [PubMed: 3004664]

Gerfen CR. The neostriatal mosaic: compartmentalization of corticostriatal input and striatonigral output systems. Nature 1984;311:461–464. [PubMed: 6207434]

Graybiel AM. Building action repertoires: memory and learning functions of the basal ganglia. Curr Opin Neurobiol 1995;5:733–741. [PubMed: 8805417]

Graybiel AM, Ragsdale CW Jr. Histochemically distinct compartments in the striatum of human, monkeys, and cat demonstrated by acetylthiocholinesterase staining. Proc Natl Acad Sci U S A 1978;75:5723–5726. [PubMed: 103101]

Graziano A, Jones EG. Widespread thalamic terminations of fibers arising in the superficial medullary dorsal horn of monkeys and their relation to calbindin immunoreactivity. J Neurosci 2004;24:248–256. [PubMed: 14715957]

Groves PM, Martone M, Young SJ, Armstrong DM. Three-dimensional pattern of enkephalin-like immunoreactivity in the caudate nucleus of the cat. J Neurosci 1988;8:892–900. [PubMed: 3346727]

Jerng HH, Pfaffinger PJ, Covarrubias M. Molecular physiology and modulation of somatodendritic A-type potassium channels. Molecular and Cellular Neuroscience 2004;27:343–369. [PubMed: 15555915]

Johnston JG, Gerfen CR, Haber SN, van der Kooy D. Mechanisms of striatal pattern formation: conservation of mammalian compartmentalization. Brain Res Dev Brain Res 1990;57:93–102.

Jones, EG. The Thalamus. Vol. Second. Cambridge University Press; 2007.

Jones EG, Hendry SHC. Differential calcium binding protein immunoreactivity distinguishes two classes of relay neurons in monkey thalamic nuclei. Eur J Neurosci 1989;1:222–246. [PubMed: 12106154]

Linden JF, Schreiner CE. Columnar transformations in auditory cortex? A comparison to visual and somatosensory cortices. Cereb Cortex 2003;13:83–89. [PubMed: 12466219]

Livingstone MS, Hubel DH. Anatomy and physiology of a color system in the primate visual cortex. J Neurosci 1984;4:309–356. [PubMed: 6198495]

Manley MS, Young SJ, Groves PM. Compartmental organization of the peptide network in the human caudate nucleus. J Chem Neuroanat 1994;7:191–201. [PubMed: 7531455]

Martin LJ, Blackstone CD, Huganir RL, Price DL. The striatal mosaic in primates: striosomes and matrix are differentially enriched in ionotropic glutamate receptor subunits. J Neurosci 1993;13:782–792. [PubMed: 7678861]

Meijering E, Jacob M, Sarria JCF, Steiner P, Hirling H, Unser M. Design and validation of a tool for neurite tracing and analysis in fluorescence microscopy images. Cytometry A 2004;58:167–176. [PubMed: 15057970]

Menegola M, Misonou H, Vacher H, Trimmer JS. Dendritic A-type potassium channel subunit expression in CA1 hippocampal interneurons. Neuroscience 2008;154:953–964. [PubMed: 18495361]

Menegola M, Trimmer JS. Unanticipated region- and cell-specific downregulation of individual KChIP auxiliary subunit isotypes in Kv4.2 knock-out mouse brain. J Neurosci 2006;26:12137–12142. [PubMed: 17122038]

Mikula S, Trotts I, Stone JM, Jones EG. Internet-enabled high-resolution brain mapping and virtual microscopy. NeuroImage 2007;35:9–15. [PubMed: 17229579]

Mountcastle VB. The columnar organization of the neocortex. Brain 1997;120:701–722. [PubMed: 9153131]

O'Kusky JR, Nasir J, Cicchetti F, Parent A, Hayden MR. Neuronal degeneration in the basal ganglia and loss of pallido-subthalamic synapses in mice with targeted disruption of the Huntington's disease gene. Brain Res 1999;818:468–479. [PubMed: 10082833]

Penny GR, Wilson CJ, Kitai ST. Relationship of the axonal and dendritic geometry of spiny projection neurons to the compartmental organization of the neostriatum. J Comp Neurol 1988;269:275–289. [PubMed: 2833538]

Prensa L, Giménez-Amaya JM, Parent A. Chemical heterogeneity of the striosomal compartment in the human striatum. J Comp Neurol 1999;413:603–618. [PubMed: 10495446]

Ragsdale CW Jr, Graybiel AM. Compartmental organization of the thalamostriatal connection in the cat. J Comp Neurol 1991;311:134–167. [PubMed: 1719043]

Rasband, WS. ImageJ. National Institutes of Health; Bethesda, Maryland, USA: 1997. http://rsb.info.nih.gov/ij

Rhodes KJ, Carroll KI, Sung MA, Doliveira LC, Monaghan MM, Burke SL, Strassle BW, Buchwalder L, Menegola M, Cao J. KChIPs and Kv4 a Subunits as Integral Components of A-Type Potassium Channels in Mammalian Brain. J Neurosci 2004;24:7903–7915. [PubMed: 15356203]

Spencer R, Charman M, Wilson PW, Lawson DEM. The relationship between vitamin D-stimulated calcium transport and intestinal calcium-binding protein in the chicken. Biochem J 1978;170:93–101. [PubMed: 204303]

Strassle BW, Menegola M, Rhodes KJ, Trimmer JS. Light and electron microscopic analysis of KChIP and Kv4 localization in rat cerebellar granule cells. J Comp Neurol 2005;484:144–155. [PubMed: 15736227]

Tepper JM, Koos T, Wilson CJ. GABAergic microcircuits in the neostriatum. Trends Neurosci 2004;27:662–669. [PubMed: 15474166]

Tippett LJ, Waldvogel HJ, Thomas SJ, Hogg VM, van Roon-Mom W, Synek BJ, Graybiel AM, Faull RL. Striosomes and mood dysfunction in Huntington's disease. Brain 2007;130:206–221. [PubMed: 17040921]

Thevenaz P, Ruttimann UE, Unser M. A pyramid approach to subpixel registration based on intensity. IEEE Trans Image Process 1998;7:27–41. [PubMed: 18267377]

Treece GM, Prager RW, Gee AH. Regularised marching tetrahedra: improved iso-surface extraction. Computers & Graphics 1999;23:583–598.

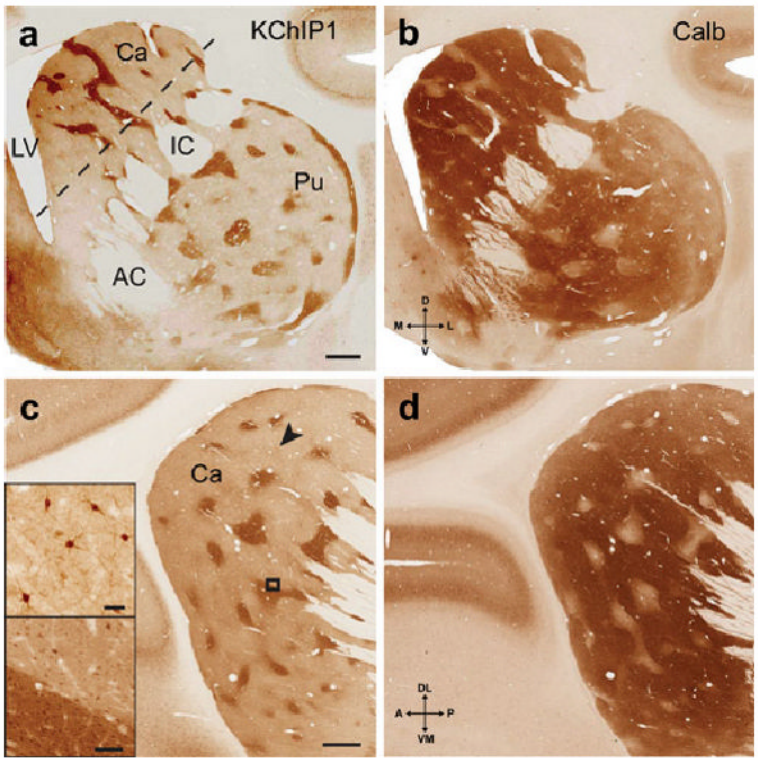

Fig. 1.

KChIP1 is a novel immunocytochemical marker for the striosomes in macaque. Coronal sections at the level of the anterior commissure showing KChIP1 immunoreactivity in the striosomes (a), with an adjacent section (b) showing immunoreactivity for calbindin in the complementary matrix compartment. In sections approximately parallel to the internal capsule (dashed line in a), a lattice-like pattern of KChIP1 immunoreactive striosomes is evident in the head of the caudate nucleus (c) with complementary staining for calbindin in an adjacent section (d). Bottom inset in c is higher magnification of box in c, and shows KChIP1immunostaining of somata in both matrix and striosomes, with heavy neuropil staining only in the striosomes. Top inset in c shows immunoreactive somata and proximal processes corresponding to the arrowhead. Scale bars: 1 mm (a and c); 40 microns (top inset in c); 100 microns (bottom inset in c). Abbreviations: AC, anterior commissure; Ca, caudate nucleus; IC, internal capsule; LV, lateral ventricle; Pu, putamen.

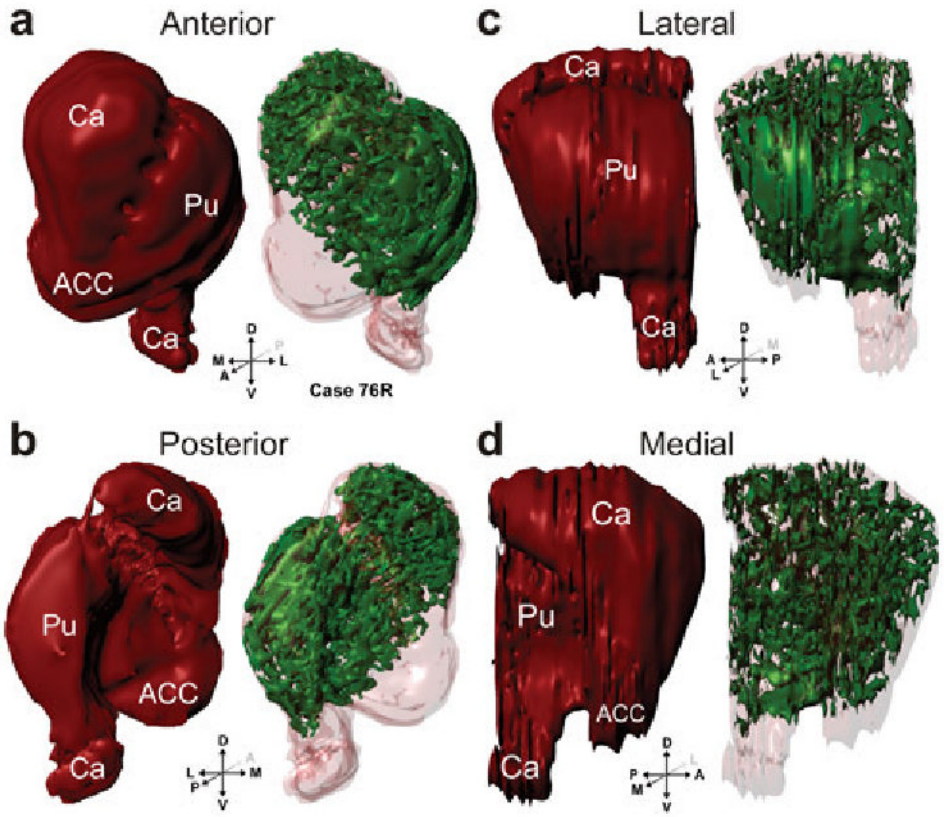

Fig. 2.

Three dimensional reconstructions of the striatum (red) and striosomes (green) from case 76R viewed in perspective, shown from anterior (a), posterior (b), lateral (c), and medial (d) views. Abbreviations: ACC, nucleus accumbens; Ca, caudate nucleus; Pu, putamen;

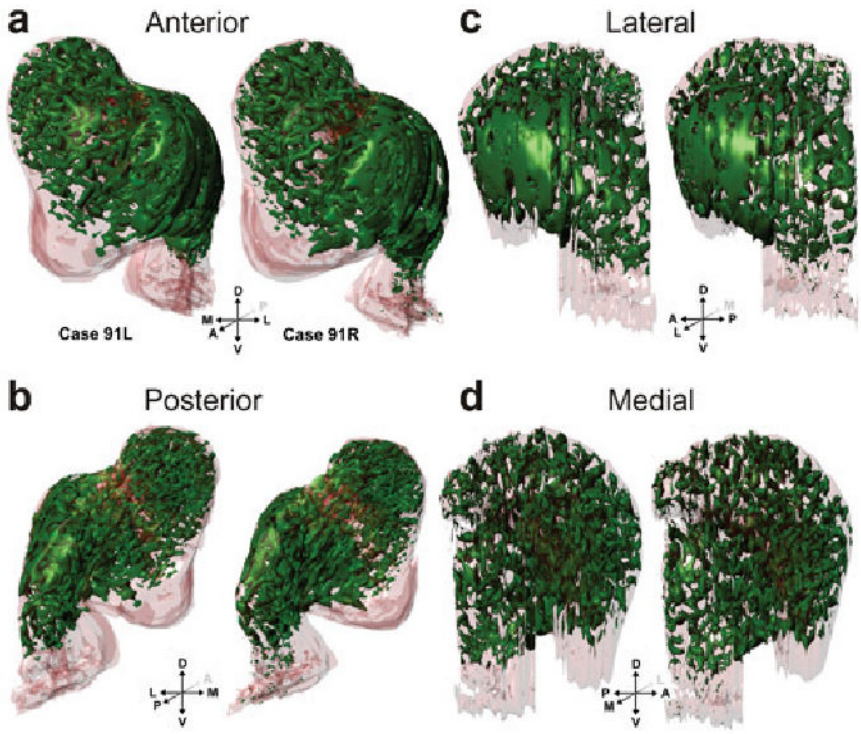

Fig. 3.

Three dimensional reconstructions of the striosomes (green) from cases 91L and 91R viewed in perspective, shown from anterior (a), posterior (b), lateral (c), and medial (d) views as in Fig. 2.

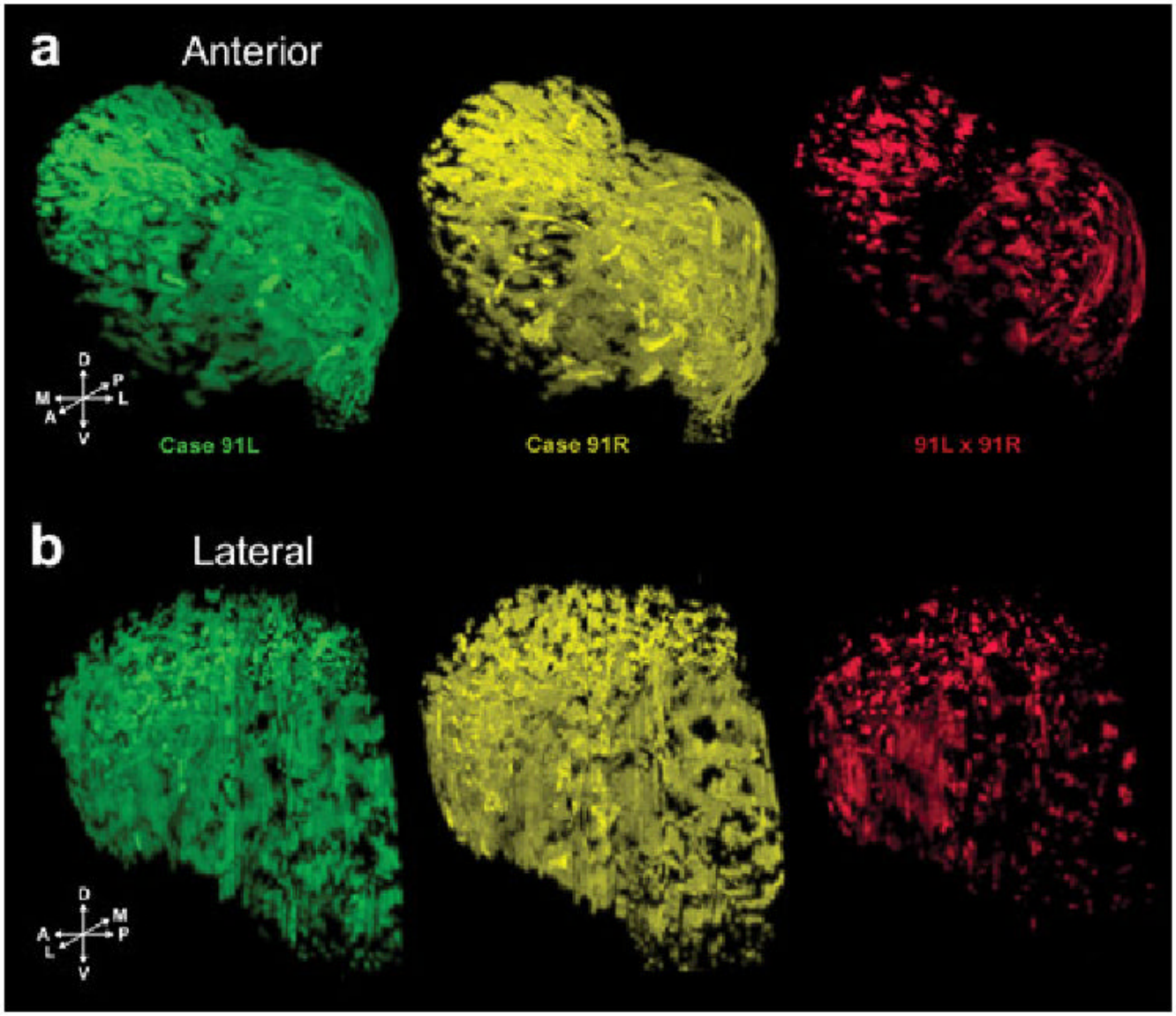

Fig. 4.

Volumetric visualization of results from spatial averaging of striosomes for cases 91L and 91R (Fig. 3). Individual striosomes from the left hemisphere (91L, green) and right hemisphere (91R, yellow), and their voxel-wise product of intensity values (91L × 91R, red). Overlap between the striosomes in the two hemispheres is 14.7% of the total individual striosomes, underscoring the spatial variability of the striosomes.

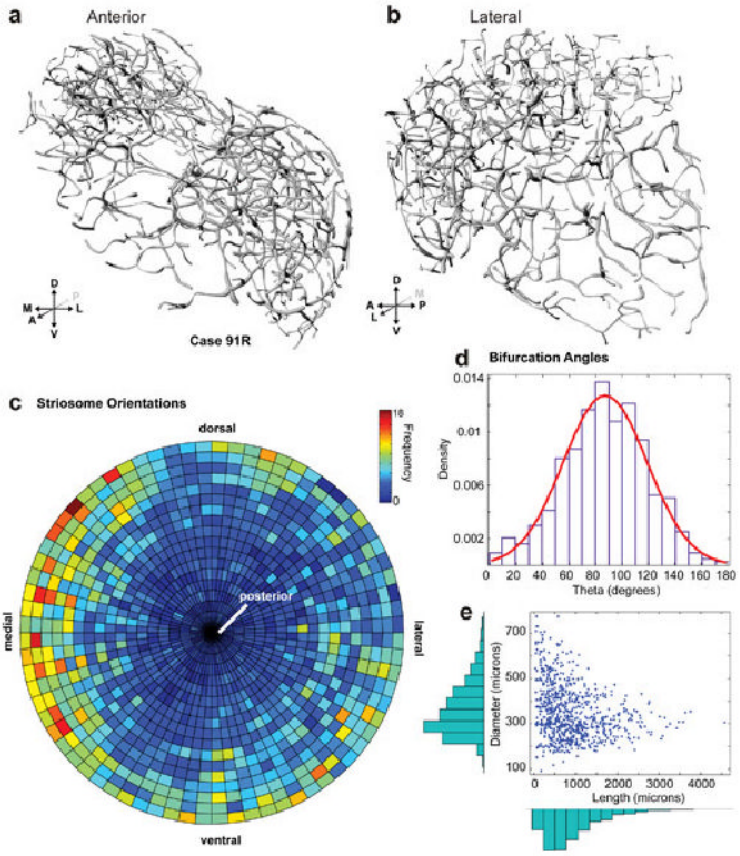

Fig. 5.

Skeletonization and morphometric analysis of case 91R from anterior (A) and lateral (B) views, with striosome segment orientations (C). Bifurcation angles (mean=87.3±31.6°, n=878) (D). Striosome diameters (mean=348.8±110.2 microns, n=776) versus lengths (mean=1045.8 ±738.7 microns, n=776) (E). Skeletonizations of other cases are shown in supplementary figs. S1, 2.

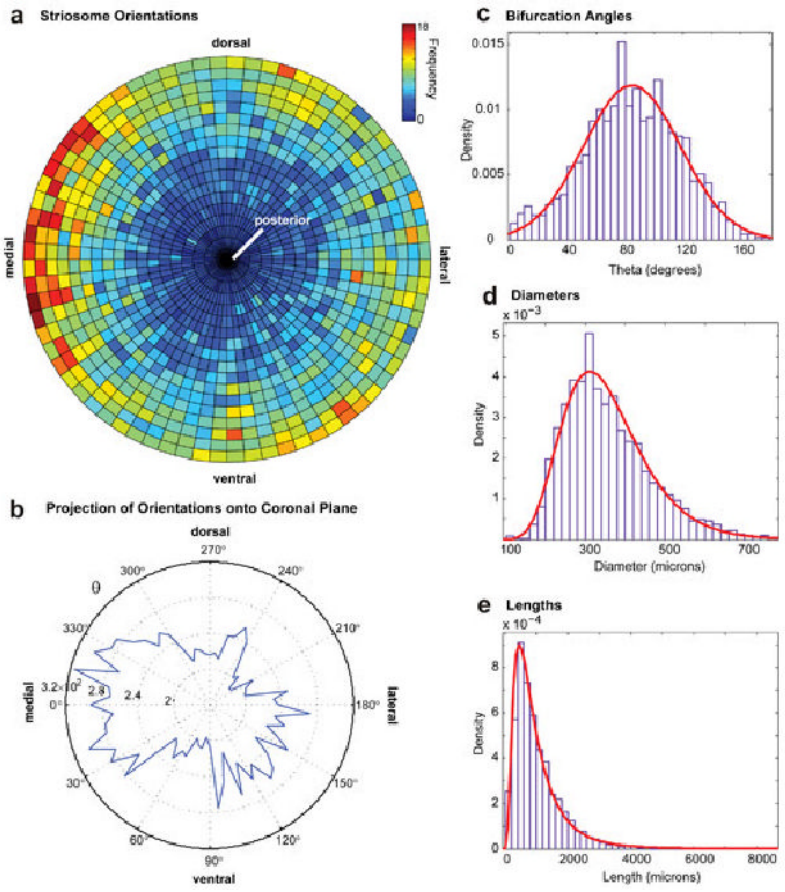

Fig. 6.

Group morphometric analyses of all three cases. Striosome segment orientations (A). Polar plot of the projection of the striosome orientations onto the coronal plane (B), showing strong medial, ventrolateral, and dorsolateral biases. Bifurcation angles (mean=84.6±33.7°, n=2764) (C). Striosome diameters (mean=355.3±108.5 microns, n=2366) (D), fit with a lognormal distribution. Striosome lengths (mean=1013.7±750.9 microns, n=2366) (E), also fit with a lognormal distribution.